Provided for non-commercial research and education use.
Not for reproduction, distribution or commercial use.

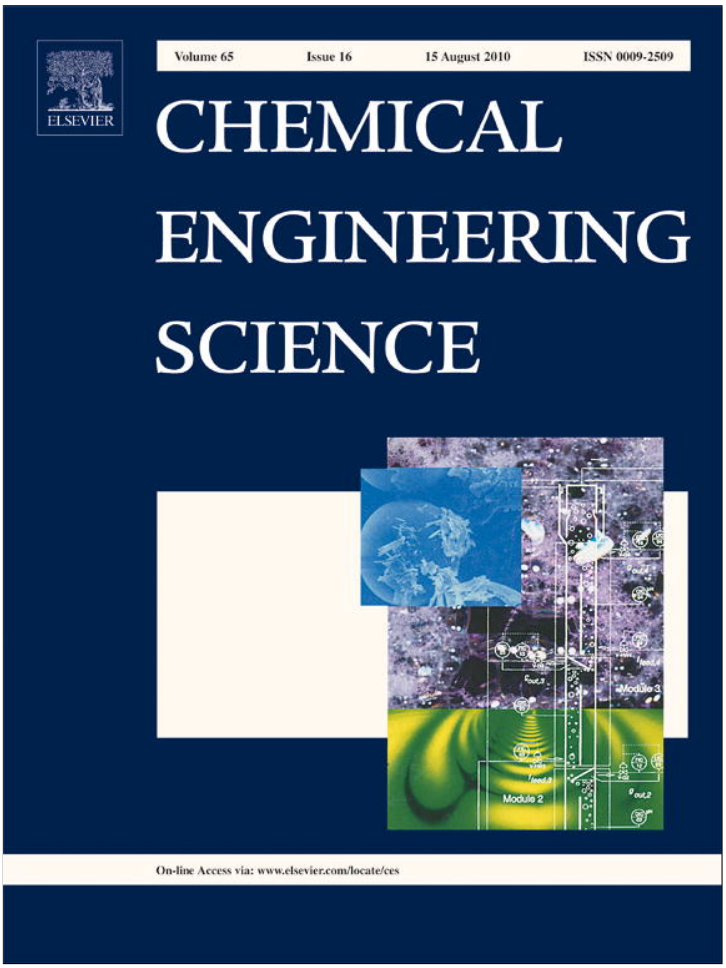

This article appeared in a journal published by Elsevier. The attached copy is furnished to the author for internal non-commercial research and education use, including for instruction at the authors institution and sharing with colleagues.

Other uses, including reproduction and distribution, or selling or licensing copies, or posting to personal, institutional or third party websites are prohibited.

In most cases authors are permitted to post their version of the article (e.g. in Word or Tex form) to their personal website or institutional repository. Authors requiring further information regarding Elsevier's archiving and manuscript policies are encouraged to visit:

http://www.elsevier.com/copyright

Author's personal copy

Chemical Engineering Science 65 (2010) 4803–4815

Contents lists available at ScienceDirect

Chemical Engineering Science

journal homepage: www.elsevier.com/locate/ces

Bacterial aerosol neutralization by aerodynamic shocks using an impactor system: Experimental results for *B. atropheus* spores

P.R. Sislian [a], J. Rau [a], X. Zhang [a], D. Pham [c], M. Li [b], L. Mädler [c], P.D. Christofides [a,d,*]

[a] Department of Chemical and Biomolecular Engineering, University of California, Los Angeles, CA 90095, USA
[b] Department of Chemical and Materials Engineering, California State Polytechnic University, Pomona, CA 91768, USA
[c] Foundation Institute of Materials Science, Department of Production Engineering, University of Bremen, Badgasteiner Str. 3, 28359 Bremen, Germany
[d] Department of Electrical Engineering, University of California, Los Angeles, CA 90095, USA

ARTICLE INFO

Article history:
Received 6 April 2010
Received in revised form
16 May 2010
Accepted 20 May 2010
Available online 1 June 2010

Keywords:
Bacterial aerosol
Aerodynamic shocks
Impactor
Computational modeling
Bacterial break-up
Aerosol collection

ABSTRACT

Neutralization of spore aerosol releases is critical in countering bioterrorism. As a possible spore aerosol neutralization method that avoids the use of chemicals, we investigate the mechanical instabilities of the bacterium cell envelope in air as bacteria are passed through aerodynamic shocks. To carry out this fundamental investigation, an experimental impactor system is used to collect the spores after they pass through a controlled shock, and a detailed computational study is carried out to determine the impactor operating conditions that lead to bacterial break-up. Specifically, the bacteria experience relative deceleration because of sharp velocity changes in the aerodynamic shock created in the experimental impactor system. Computational model results indicate that *B. atropheus* spores require a critical acceleration of $3.9-16\times10^9\,m/s^2$ compared to $3.0\times10^8\,m/s^2$ for vegetative *E. coli* to break-up consistent with our experimental findings. Our experimental results indicate that the fraction of cells surviving an aerodynamic shock with a maximum acceleration of $5.9\times10^9\,m/s^2$ is $f_l=0.030\pm0.010$.

© 2010 Elsevier Ltd. All rights reserved.

1. Introduction

Characteristics of a bacterial cell, such as degree of hydration, growth medium (e.g., agar versus broth), Gram stain (+ve versus −ve), and metabolic state (vegetative versus spore) affect its survival (Stuart and Wilkening, 2005; Tang, 2009). Survival rates of different bacterial cells are also affected by exposure to different air environments (Stuart and Wilkening, 2005; Tang, 2009). Temperature, relative humidity, ultraviolet light, and atmospheric pollutants are some factors that contribute to cell viability loss. These environmental factors minimally injure spores compared to both Gram-negative and Gram-positive vegetative cells. Intentionally disseminating spores such as *Bacillus anthracis* (anthrax) can cause much greater harm than their vegetative forms because of their extended survival in air. Consequently, it is critical to study the effectiveness of neutralization techniques on spores for defense applications.

Assuming that the detection of these agents is possible, current methods are not effective in neutralizing the aerosol cloud at its source and mostly include containment of the aerosol release in order to minimize human exposure. These methods are limited to indoor environments and employ techniques such as high efficiency particulate air (HEPA) filtration, electrostatic precipitation, steam condensation, ultraviolet (UV) inactivation as well as diverting airflows (Vitko, 2005).

As an alternative to these methods, aerodynamic shocks provide a mechanical mechanism of neutralizing bacterial aerosols and can be applied at the point of their release. Previous work has shown that shocks can reduce the viability of bacteria in suspensions and in powder form (Horneck et al., 2001; Lundbeck and Skoldber, 1963; Teshima et al., 1995). Our computational and theoretical work has shown that aerodynamic shocks cause vegetative bacterial aerosol to break-up (Sislian et al., 2010, 2009). Aerodynamic shocks are characterized by sharp changes in fluid properties (velocity, temperature, pressure). Due to its inertia, the bacterium cannot adjust to the sharp drop in velocity; therefore, it decelerates relative to the gas flow-field. When the relative deceleration reaches a critical value the cell breaks-up (Chandrasekhar, 1961; Joseph et al., 1999; Sislian et al., 2010, 2009). An impactor system has been built and modeled to achieve different bacterial accelerations through a well-defined aerodynamic shock (see Section 2.1.2) (Sislian et al., 2010, 2009). After passing through the shock, the bacterial aerosol is collected at low velocity ($<10\,m/s$) to avoid break-up at the point of impaction

* Corresponding author at: Department of Chemical and Biomolecular Engineering, University of California, Los Angeles, CA 90095, USA.
Tel.: +1 310 794 1015; fax: +1 310 206 4107.
E-mail address: pdc@seas.ucla.edu (P.D. Christofides).

0009-2509/$ - see front matter © 2010 Elsevier Ltd. All rights reserved.
doi:10.1016/j.ces.2010.05.035

Author's personal copy

(Stewart et al., 1995). Gram-negative *Escherichia coli* vegetative cells break-up at decelerations $>3.0\times10^8\,m/s^2$ (Sislian et al., 2010, 2009). In previous work, the impactor was operated to reach computed decelerations of $5.0\times10^9\,m/s^2$ which predict break-up of the cells. The experimentally measured fraction of cells remaining alive was 0.035 ± 0.012, confirming the computational predictions.

This study focuses on the effect of aerodynamic shocks on spores which are more relevant as bioterrorism threats. In laboratory settings, *Bacillus subtilis* var. *niger*, reclassified as *Bacillus atropheus* (Fritze and Pukall, 2001), is suggested as a surrogate for *B. anthracis* that emulates the spore's physical characteristics but avoids its pathogenicity (Fitch, 2005). The two spores have similar surface tension values (Chen et al., 2010). Both computational and experimental methods are used to study the effect of aerodynamic shocks on *B. atropheus* spores and to obtain the fraction of cells that remain alive after the effect of impactor operation (f_I).

2. Experimental materials and methods

2.1. Experimental setup

The experimental system discussed in previous work (Sislian et al., 2010) is used to determine the effect of the aerodynamic shock on *B. atropheus* spores. The details of the system (see Fig. 1) are described below. The vegetative *E. coli* suspension was substituted with *B. atropheus* spore suspension (see Section 2.2) in the nebulizer (see Section 2.1.1) (Sislian et al., 2010). The resulting aerosol travels to the impactor which was operated at different downstream to upstream pressure ratios (see Section 2.1.2). Quantitative analysis of the survival rate was carried out using fluorescence flow cytometry (see Section 2.3).

2.1.1. Nebulization

The *B. atropheus* spores suspension (see Section 2.2) was fed via a syringe pump (KDS410, Kd Scientific) at a liquid flow rate $Q=0.05$ mL/min for 20 min to a capillary nebulizer (TR-30-A1, Meinhard Glass Products). Nitrogen (N_2) gas was supplied at a critical flow rate of 0.2 L/min through the annular region. The liquid was fed at a specified bacterial concentration (see Section 2.2) determined by the optical density measurement at 600 nm (OD_{600}). Nitrogen was supplied to the nebulizer at a pressure P_n via a pressurized tank. In all the experiments, the nebulizer was operated at $Q=0.05$ mL/min, $OD_{600}=0.5$, and $P_n=2$ atm. The spore concentration at $OD_{600}=0.5$, as measured using fluorescence flow cytometry (see Section 2.3), was $5.02\pm1.24\times10^5$ spores/mL. The average expected nebulized droplet size is 10 μm, which translates to approximately 1 cell in every 1000 droplets assuming no aggregates are formed in the droplets.

2.1.2. Impactor system

A detailed description of the impactor system was given in a previous work (Sislian et al., 2009, 2010). Briefly, the impactor system consists of a plate designed for the collection of the bacterial aerosol (see Fig. 1; parts 4 and 5) which is placed perpendicular to the gas flow emerging from a converging nozzle (see Fig. 1; part 3). Isentropic flow theory of an ideal gas predicts a critical downstream (P_1) to upstream (P_0) pressure ratio (χ_{crit}) below which the flow at the exit of the nozzle is sonic (Liepmann and Roshko, 2001; Shapiro, 1953). For Nitrogen (N_2), χ_{crit} is 0.53 (Sislian et al., 2009, 2010). The generated impinging flow on a plate from a converging nozzle operating under sonic conditions results in the creation of a standoff shock whose properties can be changed by varying impactor geometry (distance between nozzle and plate x and diameter of nozzle d) and operating conditions (Alvi et al., 2002; Delamora et al., 1990, 1990; Jurcik et al., 1989; Powell, 1988; Sislian et al., 2009). The deceleration tube (see Fig. 1; parts 4 and 5) is filled with 600 μL of phosphate buffer saline (PBS) solution (BP2438-4, Fisher Scientific), which keeps the liquid level to about 4 mm away from the entrance of the

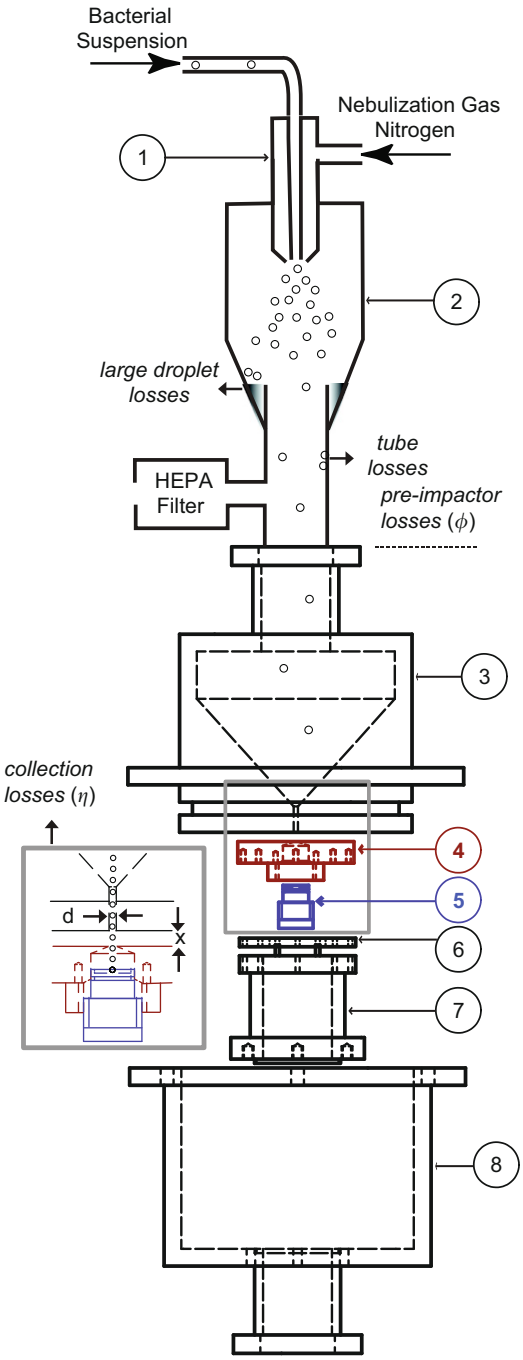

Fig. 1. Schematic of the experimental system. (1) Meinhard nebulizer with a concentric nozzle mixing a liquid bacterial suspension feed and a dispersion gas (N_2), (2) nebulization chamber to collect large droplets, (3) converging nozzle with an exit diameter of $d=0.5$ mm, (4) and (5) a flat surface with a 0.5 mm hole combined with a screw that accommodates the collection substrate make up the deceleration tube, (6) 1.4 mm spacer fixes the spacing x between the impactor and nozzle to 0.6 mm, (7) support holding the deceleration tube and a flat surface at fixed distance from the nozzle, and (8) exit chamber. Major losses in the experimental system are shown in italic.

Author's personal copy

deceleration tube. The plate to nozzle distance is set at $x/d=1.2$. The impactor system is operated at an upstream pressure of $P_0=1$ atm with three different pressure ratios $\chi=P_1/P_0=0.98$, 0.50 and 0.11 for 20 min. After each experimental run the volume of PBS remaining in the deceleration tube was measured and used in mass balance calculations to determine the fraction of cells surviving the impactor operating conditions (see Section 4). Fig. 1 shows the losses, ϕ and η, of bacterial particles in different parts of the experimental system which are discussed in Sections 2.1.3 and 3.2.2.

2.1.3. Particle losses in experimental setup

Losses of spores to the walls of the system before entering the impactor $(1-\phi)$ were accounted for using calculations developed in our previous work (Sislian et al., 2010). Specifically, vegetative *E. coli* cells were collected on an in-line filter placed before the impactor system (Sislian et al., 2010). Fluorescence microscopy images were taken to count the fluorescent bacteria on the stained filter. These images were then analyzed to calculate the fraction of cells entering the impactor (ϕ), which is defined as

$$\phi=\frac{n_i}{n_n} \tag{1}$$

where n_n is the total number of cells nebulized and n_i is the total number of cells entering the impactor. The parameter ϕ was calculated to be 0.088 ± 0.029 from the in-line filter counts (Sislian et al., 2010). Although the calculation was made using experimental data on *E. coli* vegetative bacteria (whose diameter is $\approx1\,\mu$m), the same value of ϕ was used for *B. atropheus* spores (whose diameter is $\approx0.5\,\mu$m). Two processes are responsible for losses in the system before the impactor: (1) losses of large nebulized liquid droplets on the nebulization chamber (see Fig. 1; part 2) walls, and (2) losses of bacterial aerosol in the tubes leading to the impactor. Losses in the tubes can either be diffusional or inertial (impaction). Diffusional losses $(1-n_{out}/n_{in})$ were calculated for circular tubes using the following expression (Hinds, 1999):

$$n_{out}/n_{in}=1-5.5\left(\frac{DL}{Q_g}\right)^{2/3}+3.77\left(\frac{DL}{Q_g}\right) \tag{2}$$

where n_{out} and n_{in} are the number of particles exiting and entering the tube, respectively, D is the diffusion coefficient, L is the length of the tube, and Q_g is the volumetric flow rate of gas. For both 1 and 0.5 μm particles the ratio, n_{out}/n_{in}, is calculated to be $>99\%$. Therefore, diffusional losses $(1-n_{out}/n_{in})$ are negligible. To calculate the impaction losses the following relation was used (Hinds, 1999):

$$n_{out}/n_{in}=1-2\theta\left(\frac{\rho_p d_p^2 U_g}{18\mu_g D_s}\right) \tag{3}$$

where ρ_p is the particle density, d_p is the particle diameter, U_g is the average gas velocity in the tubes leading to the impactor, μ_g is the gas viscosity, D_s is the tube diameter and θ is the bend angle in radians. The term in parentheses in Eq. (3) is also referred to as the Stokes number. The ratio, n_{out}/n_{in}, was also $>99\%$ for both particle sizes. Therefore, most of the losses before the impactor $(1-\phi)$ are attributed to the identical nebulization process (see Section 2.1.1)) for $\approx1\,\mu$m *E. coli* vegetative cells and $\approx0.5\,\mu$m *B. atropheus* spores under identical conditions with $\phi=0.088\pm0.029$.

2.2. Spore preparation

Bacillus atropheus (strain ATCC 9372) was used as the standard bacterial aerosol to study the aerodynamic shock effect on bacterial spores in the impactor system. In our previous study, *E. coli* was used as a test aerosol for vegetative bacterial cells (Sislian et al., 2010). The methods described in this section were adopted with minor modifications to the standard procedures for culturing and washing of *Bacillus* spores (Harwood and Cutting, 1990). All vegetative cultures were initiated from a stock *B. atropheus* suspension (80% glycerol solution) stored at $-20\,^{\circ}$C. Nutrient broth (Fisher) of 5 mL was inoculated with 10 μL of stock suspension in a test tube. The vegetative culture was incubated in a shaker (Excella E24, New Brunswick Scientific) at 32 °C and 200 rpm for approximately 22–25 h. To start the spore culture, 1 mL of the vegetative *B. atropheus* was inoculated in 15 mL of $2\times$ SG media that was prepared as described in standard procedures (Harwood and Cutting, 1990). The spore culture was incubated for 12 days at 32 °C and 200 rpm, allowing time for the cells to exhaust nutrients in the medium, thereby inducing sporulation.

After the incubation period the spore culture was washed over 4 days. On day 1, the culture was centrifuged at 4400 rpm for 15 min (Centrifuge 5702, Eppendorf). Three layers were observed with the lower layer containing the free spores and the top two layers containing cell debris (Harwood and Cutting, 1990). The suspension was washed three times with cold autoclaved deionized (DI) water, keeping all three layers and then shaking in an ice bath overnight. Similar procedures were repeated for days 2 and 3 with the exception of resuspending and decanting the top two layers instead of keeping them. Most of the cell debris layers were removed after the third day. On day 4 the suspension was centrifuged at 4400 rpm and washed three times using cold PBS. The optical density of the spore suspension was measured at a wavelength of 600 nm (OD_{600}) using a visible light spectrophotometer (Genesis 20, Thermo Scientific) before storage at 4 °C.

To check the degree of sporulation, starting suspensions were treated with lysozyme, which breaks down the peptidoglycan outer membrane in Gram-positive vegetative cells such as *B. atropheus*. Since spores do not have an exposed peptidoglycan layer, lysozyme is expected to have no effect. The suspension was diluted to $OD_{600}=0.05$ and lysozyme (L6876, Sigma Aldrich) was added for a solution concentration of 2.8×10^{-1} mg/mL and incubated for 30 min at 32 °C and 200 rpm. The lysozyme treatment was also used on vegetative *B. atropheus*. The fraction of spores was determined by comparing viability analysis (see Section 4.1.1) of the spore suspension to the vegetative cells.

At the start of each experiment, a positive and a negative control were prepared by diluting the spore suspension to $OD_{600}=0.05$. The positive control was incubated in a water bath at 100 °C for over 2 h to neutralize the spores (Cortezzo et al., 2004). The negative control was left untreated and is therefore expected to have the highest concentration of viable spores. The samples collected after the impactor operation are compared to both the positive and negative control to assess the effect of the shock (see Section 4.2).

2.3. Bacterial viability analysis

Bacterial viability is determined using LIVE/DEAD® *Bac* Light™ (cat. number L7012; Life Technologies Corporation) (Berney et al., 2007; Laflamme et al., 2004). The assay contains two components: (A) 3.34 mM STYO 9, a green-fluorescent nucleic acid stain, in dimethyl sulfoxide (DMSO) and (B) 20 mM propidium iodide (PI), a red-fluorescent nucleic acid stain, in DMSO. STYO 9 penetrates both intact and damaged membranes, while PI only penetrates damaged membranes. A stock dye solution is prepared at the start of every experiment by mixing 5 μL of each of components A and B with 10 μL deionized water (DI). All controls and experimental samples mentioned in Sections 2.1 and 2.2 were stained with the

Author's personal copy

stock dye solution to a final concentration of 8.35 and 50 μM of STYO 9 and PI, respectively.

The stained samples were analyzed using a fluorescence flow cytometer (FACScan^{TM}, BD Biosciences). The cytometer was operated at 12 μL/min for 20 s with a 488 nm excitation laser. Red fluorescence was measured with a high pass filter at 630 nm (FL2-H) and green fluorescence was measured with a bandpass filter of 520 nm (FL1-H). The forward scatter (FSC) and side scatter (SSC) were also measured for the particles passing the laser. Photomultiplier tubes were used to amplify the optical signal for FL1-H, FL2-H and SSC at 730, 648 and 462 V, respectively. A photodiode was used to detect the FSC signal.

3. Computational results

3.1. Gas flow field

At low aerosol concentrations, the equations for gas and particle dynamics are one-way coupled (Friedlander, 2000). First, the gas dynamics equations are solved and the gas velocity is used to calculate the particle dynamics. The FLUENT® computational fluid dynamics (CFD) code was developed to solve both gas and particle dynamics in the experimental impactor system of Fig. 1 (Sislian et al., 2009). The Reynolds time-averaged Navier–Stokes equations in Cartesian tensor form are solved (for a detailed discussion the reader is referred to Sislian et al., 2009 and Sislian et al., 2010). To achieve closure of the Navier–Stokes equations, the Reynolds stress term is calculated using the Boussinesq hypothesis (Hinze, 1975). A standard $k-\varepsilon$ turbulence model is used in the gas flow equations. A detailed computational parametric study indicated that the maximum centerline Mach number (M_{max} increases with increasing x/d and decreasing P_1/P_0) (Sislian et al., 2009). Furthermore, at higher x/d (>1.4) the aerodynamic shock is unstable (Sislian et al., 2009). $x/d=1.2$ had the highest M_{max} with no flow instabilities (Sislian et al., 2009). Operating the impactor at three different pressure ratios $\chi=0.98$, 0.50, and 0.11 captures gas flow fields with no aerodynamic shock, at critical nozzle flow (χ_{crit}), and strong aerodynamic shock, respectively. The maximum centerline Mach number is 2.36 at $\chi=0.11$ (see Table 1).

3.2. Particle dynamics

The velocity profile of the particle motion is used for the calculation of mechanical forces induced on the particle (see Section 3.2.1). As in previous work, the particle trajectory is solved using Newton's second law with the gas flow field solutions from Section 3.1 (Sislian et al., 2010, 2009)

$$m_p \frac{dv_p}{dt} = \frac{1}{2} C_D \rho_g A_p (v_g - v_p)|v_g - v_p|, \tag{4a}$$

$$\frac{dx}{dt} = v_p, \tag{4b}$$

where v_p and v_g are the velocity of the bacterial particle and gas, respectively, m_p is the mass of the particle, ρ_g is the density of the gas, A_p is the projected area of the bacterium on the plane perpendicular to the flow direction, and C_D is the drag coefficient. The thermophoretic, gravitational, and Basset history term are neglected in Eq. (4a). The drag force is assumed to be the major force acting on the bacterial particle which is typical for impactor systems. A high Mach number drag law is used to calculate the drag coefficient (C_D) (Clift et al., 1978). The size of *bacillus* spores is in the range of 0.5−1.2 μm (Conn, 1930; Chen et al., 2010). The bacterium is simulated as a 0.5 μm sphere with a density ρ_p of 1 mg/mL which is representative of values reported in the literature (Laskin and Lechevalier, 1974; Willeke and Baron, 2001). Values for 1 μm particles were obtained from previous studies (Sislian et al., 2010). The computational simulations mimic the experimental conditions in the study with $x/d=1.2$ under shock ($\chi=0.11$,0.50) and non-shock ($\chi=0.98$) conditions. The detailed conditions are shown in Sections 3.2.1 and 3.2.2. The computational results predict the collection efficiency of the impactor system at different operating conditions (see Section 3.2.2) and bacterial envelope instability (see Section 3.3).

Table 1
Aerodynamic shock properties at different operating conditions with $x/d=1.2$ and $P_0=1$ atm.

χ	M_{max}	Re
0.98	0.14	9.9×10^2
0.50	0.96	5.8×10^3
0.11	2.36	5.4×10^3

3.2.1. Particle acceleration

A fifth-order Runge–Kutta method is used to numerically integrate Eqs. (4a) and (4b) using the gas velocity obtained from the computational model described in Section 3.1. The particle velocity is calculated every $5\times10^{-5}-10^{-7}$ m (for $\chi=0.11-0.98$) along the centerline of the impactor. Fig. 2 shows the gas and particle velocity profiles along the centerline of the impactor in the region of the shock. Under shock conditions ($\chi=0.11$), the aerodynamic shock is observed as a sharp drop in gas velocity (see Fig. 2-a). As the particle does not adjust to the gas stream velocity, it experiences a relative deceleration. For non-shock conditions ($\chi=0.98$), the gas velocity decreases at slower rate compared with the shock allowing the particle to adjust its velocity (Fig. 2-c) without experiencing a relative deceleration as strong as in the shock case. Fig. 2-b shows the velocity profiles for $\chi=0.50$ where the particle undergoes an intermediate relative deceleration.

The relative deceleration of the particle is determined by calculating the relative velocity derivative with respect to time (Sislian et al., 2009). The results of this differentiation, expressed in absolute values, are shown in Fig. 3. The decelerations provide a measure of the force required to neutralize bacterial aerosols (see Section 3.3). As seen in Fig. 3-b and c, the absolute value of acceleration increases at approximately 5×10^{-4} m from the nozzle exit after the main deceleration peak. Since Brownian motion and gravitational effects were neglected in Eq. (4a), particles artificially stop before reaching the collection tube bottom. This is manifested as a second increase in the absolute value of the acceleration at the entrance of the deceleration tube. In our previous work, simulations with 1 μm particles showed similar increases in the acceleration before the inlet of the deceleration tube because of assumptions in the computational model discussed in Section 3.2 (Sislian et al., 2010).

The maximum centerline decelerations (a_{max}) reached between the nozzle exit and deceleration tube entrance for the three different operating conditions are reported in Table 2. The maximum acceleration and Weber number increase with decreasing χ as expected from previous work (Sislian et al., 2010, 2009). At $\chi=0.11$, acceleration increases with smaller particle sizes, which is a trend observed for $\chi=0.14$ at $x/d=1.0$ and 1.4 in our previous work (Sislian et al., 2009). At $\chi=0.98$ and 0.50, the trend is reversed as the flow transitions to subsonic velocities.

Author's personal copy

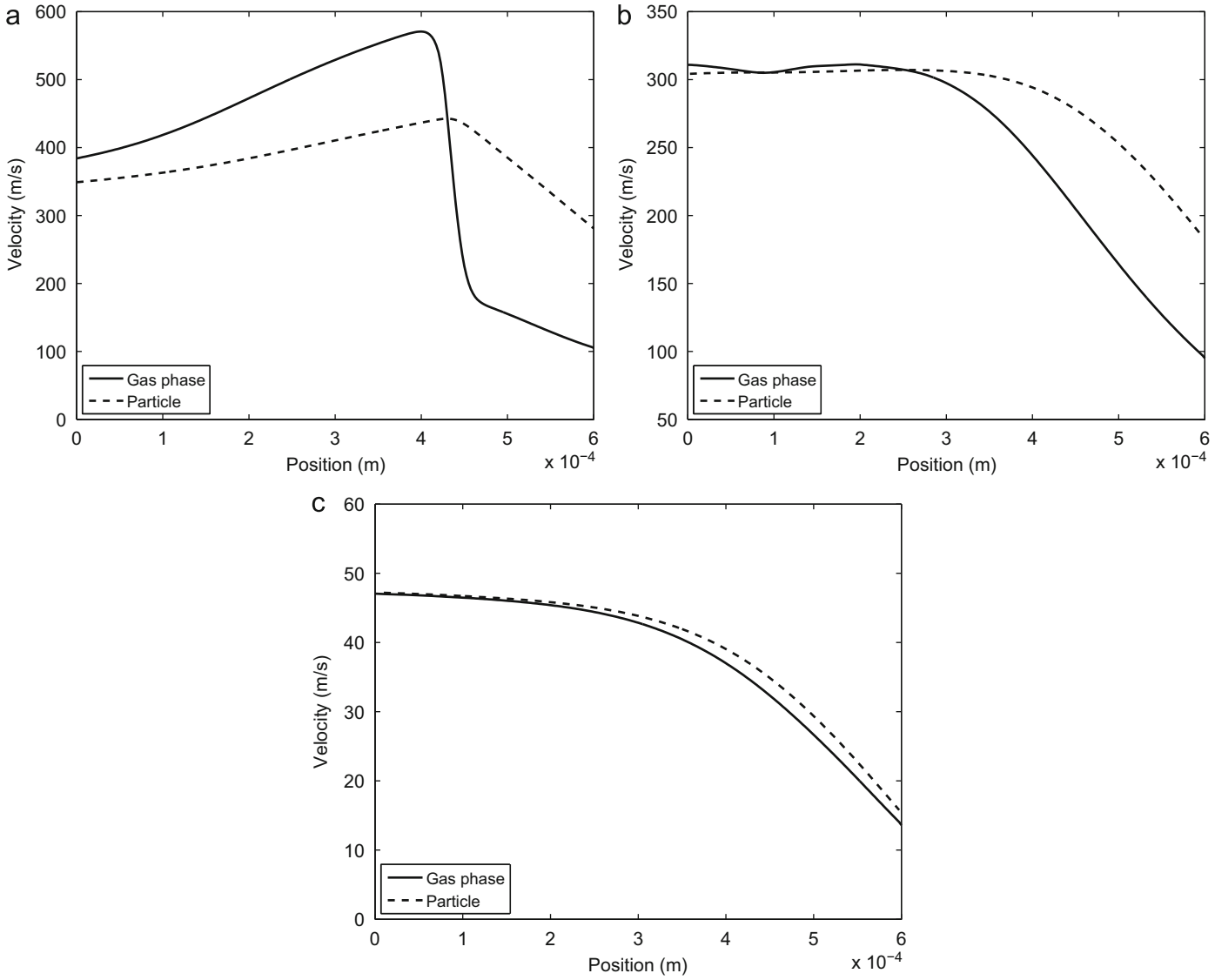

Fig. 2. Centerline particle and gas velocity as a function of the distance from the nozzle. The entrance of the collection tube is at a distance 6×10^{-4} m from the nozzle exit. Impactor operating conditions: (a) $\chi=0.11$, (b) $\chi=0.5$, and (c) $\chi=0.98$.

3.2.2. Particle collection efficiency

In Section 3.2.1, average gas velocities were used to calculate the particle acceleration. However, the collection efficiency for highly turbulent flows and low-density, small-size aerosols, depends on particle dispersion due to gas velocity fluctuations. The collection efficiency (η) is defined as the ratio of the number of particles that pass through the collection tube entrance compared to the number of particles that enter the impactor inlet. The bacterial collection efficiency (η) for all three impactor operating conditions ($\chi=0.11$,0.50,0.98) is evaluated to determine the overall bacterial aerosol neutralization rate in Section 4. The random walk model is employed to study the effect of velocity fluctuation on bacterial aerosol with reasonable computational load. Stochastic tracking of the particles is used to account for the turbulent dispersive effects in the gas flow. In the stochastic tracking model the gas velocity is represented as an average plus a fluctuating term when calculating the particle velocity, v_p, in Eq. (4a). The fluctuating velocity is kept constant for time intervals corresponding to the lifetime of turbulent eddies. The following equations describe the stochastic behavior:

$$v_g=\overline{v}+v' \tag{5a}$$

$$v'=\zeta\sqrt{\overline{v'^2}}=\zeta\sqrt{2k/3} \tag{5b}$$

$$t_L=0.15k/\varepsilon \tag{5c}$$

$$\tau_\varepsilon=-t_L\log r \tag{5d}$$

where v_g is the instantaneous gas velocity, $\overline{v}$ is the average velocity, and v' is the velocity fluctuation term. v' is a function of ζ, a normally distributed random number, and $\overline{v'^2}$ is the local root mean square of the fluctuations. $\overline{v'^2}$ is calculated based on the assumption of isotropy and is given by $\overline{v'^2}=2k/3$, with k being the turbulence kinetic energy in the $k-\varepsilon$ model. t_L is the lagrangian time interval, ε is the turbulence dissipation rate, τ_ε is the lifetime of the eddies, and r is a uniformly distributed random number between 0 and 1. Fig. 4 shows the path of five particles released from the inlet as they exit the nozzle of the impactor system for both $\chi=0.11$ (Fig. 4-a), $\chi=0.50$ (Fig. 4-b), and $\chi=0.98$ (Fig. 4-c). In calculating η, 10,000 particles are released at the inlet of the impactor. The particles are then counted as they pass the virtual surfaces $s-1$ (nozzle exit) and $s-2$ (deceleration tube entrance), shown in Fig. 5. Except for the pressure inlet and outlet,

Author's personal copy

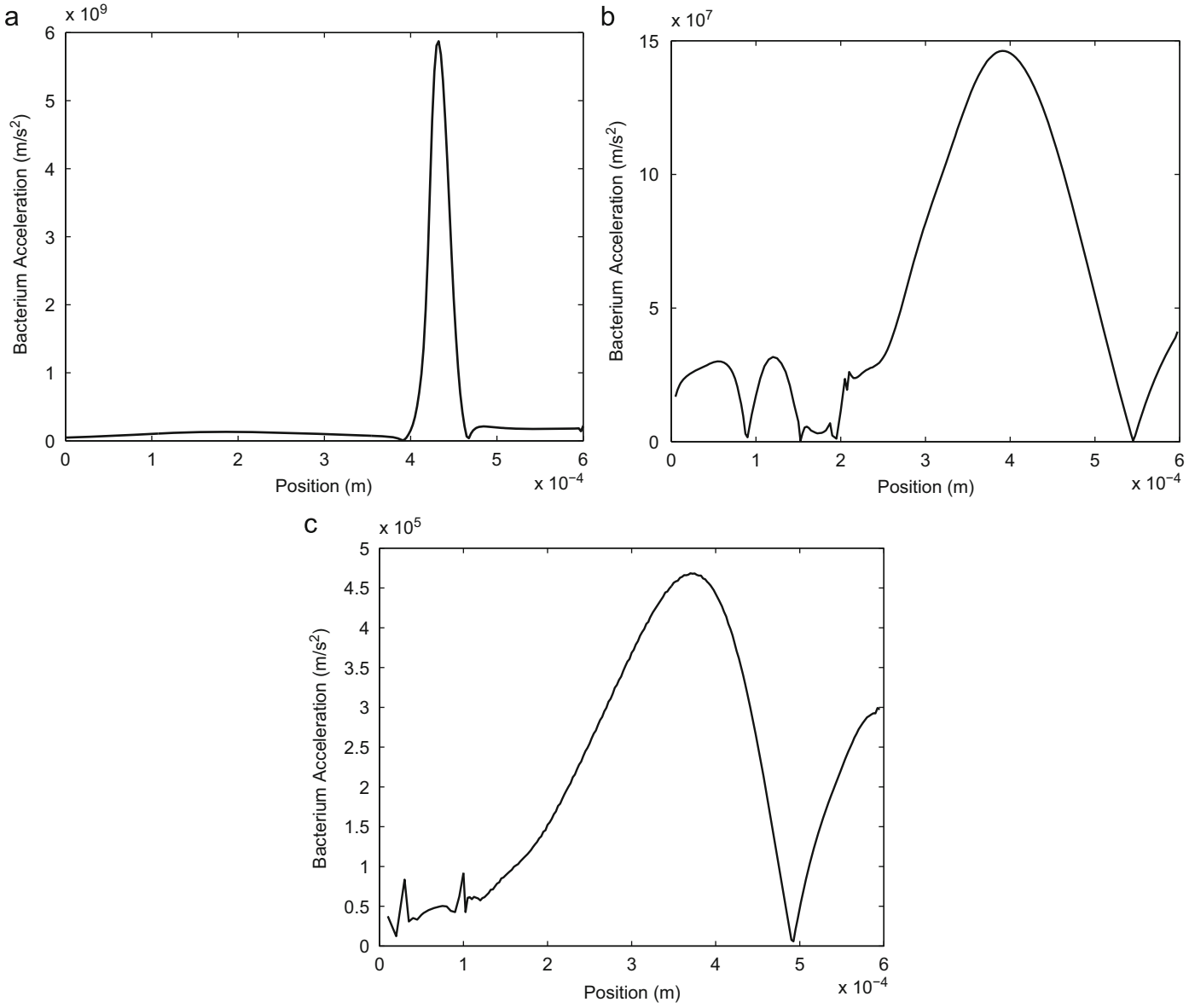

Fig. 3. Bacterial particle acceleration (relative to gas flow) as a function of the distance from the nozzle. The entrance of the collection tube is at a distance 6×10^{-4} m from the nozzle exit. Impactor operating conditions: (a) $\chi=0.11$, (b) $\chi=0.5$, and (c) $\chi=0.98$.

Table 2
Particle dynamics parameters at different operating conditions with $x/d=1.2$ and $P_0=1$ atm for $d_p=0.5$ and 1 μm.

χ	a_{max} (m/s^2)		We_{max}		η	
	0.5 μm	1 μm	0.5 μm	1 μm	0.5 μm	1 μm
0.98	4.7×10^5	1.7×10^6	5.6×10^{-4}	1.70×10^{-2}	0.26	0.35
0.50	1.5×10^8	2.0×10^8	5.4×10^{-1}	3.5×10^0	0.48	0.72
0.11	5.9×10^9	5.0×10^9	1.7×10^0	3.1×10^0	0.34	0.51

all the boundaries shown in Fig. 5 are assumed to be reflection boundaries. The collection efficiency is defined as follows:

$$\eta=\frac{n_c'}{n_i} \tag{6}$$

where n_i is the number of particles entering the impactor and n_c' is the number of particles that enter the collection tube. n_c' is calculated under the assumption of no break-up. η is used to determine the total number of live cells that would be collected if the shock were to have no effect (see Section 4). For different operating conditions, the collection efficiency (η) for both 1 and 0.5 μm size particles is reported in Table 2. The values for 1 μm are taken from our previous computational work (Sislian et al., 2010). η increases with diameter as the inertia of the particle increases and prevents it from following the gas streamlines (Hering et al., 1978, 1979).

3.3. Critical accelerations for B. atropheus

Rayleigh–Taylor instabilities are created at interface between two fluids of different density (air-bacterium) when they are at relative acceleration with respect to each other (Chandrasekhar, 1961; Joseph et al., 1999). The acceleration induces waves on the interface which become unstable at a critical acceleration of

$$a_c=4\pi^2\frac{\sigma}{\rho_p d_p^2} \tag{7}$$

where a_c is the critical acceleration, σ is the surface tension of the bacterium, d_p is the diameter of the bacterium, and ρ_p is the

Author's personal copy

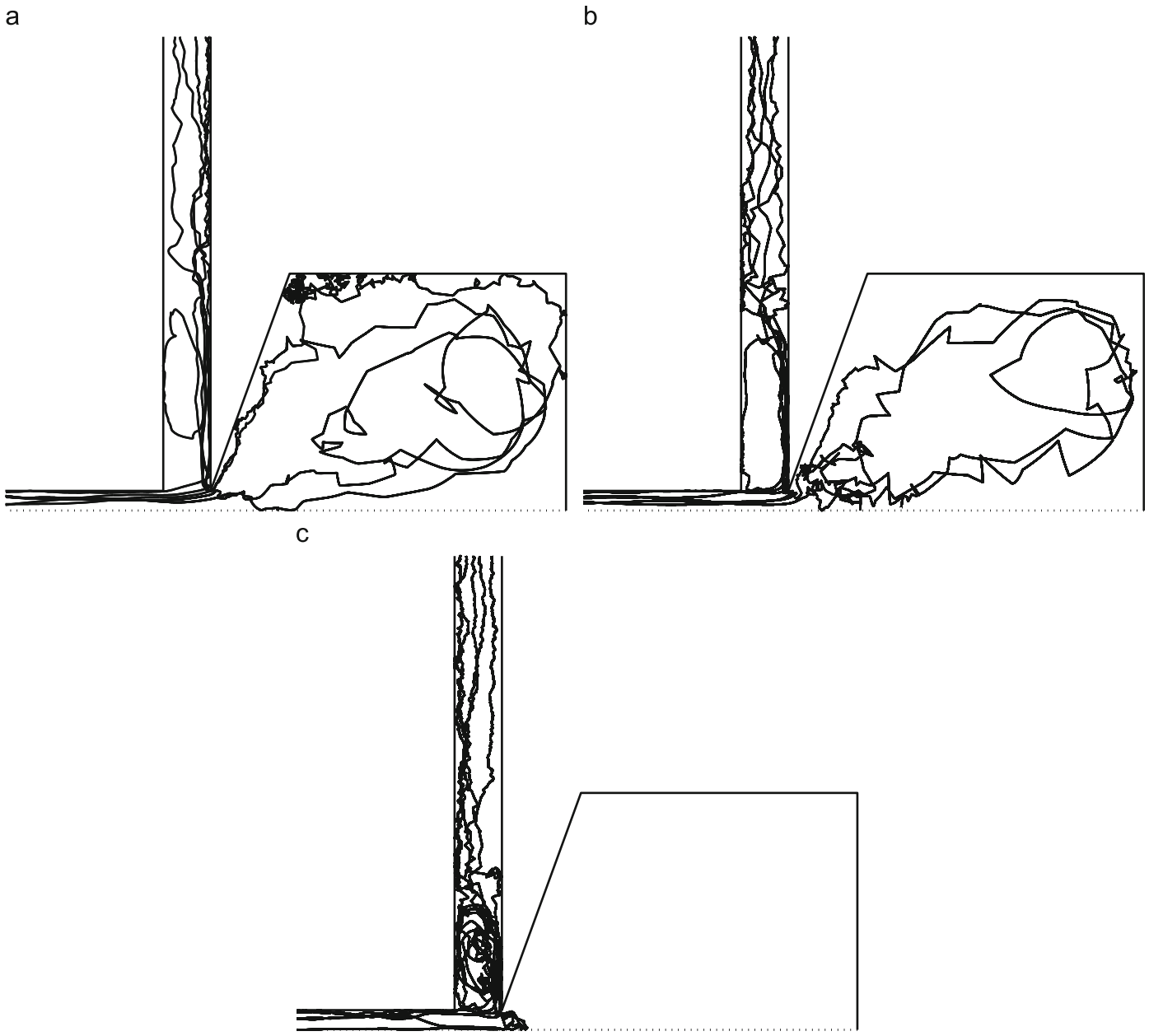

Fig. 4. Representative trajectories of five particles released from the inlet of the impactor for (a) $\chi=0.11$, (b) $\chi=0.5$, and (c) $\chi=0.98$. The collection efficiencies as measured by the number of particles entering the collection tube are 0.37, 0.48 and 0.26 for $\chi=0.11$, 0.50, and 0.98, respectively.

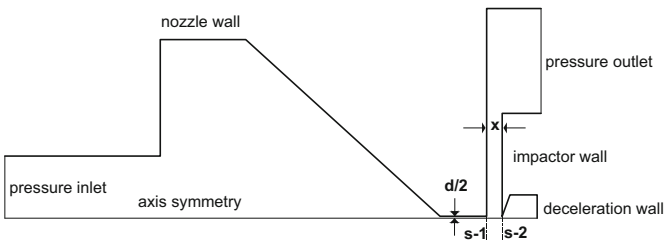

Fig. 5. Computational domain of the impactor. The two dashed lines indicate different virtual surfaces (S-1 and S-2) where particles are counted. The collection efficiency is calculated by dividing the number of particles passing S-2 by that of S-1.

density of the bacterium. The Weber number of the bacterium should also exceed the critical Weber number (Joseph et al., 1999)

$$We > We_c = 12(1+1.077Oh^{1.6}) \tag{8a}$$

where

$$We = \frac{\rho_g(v_{p_i}-v_{g_i})^2 d_p}{\sigma} \tag{8b}$$

and

$$Oh = \frac{\mu_p}{(\rho_p d_p \sigma)^{1/2}} \tag{8c}$$

where *We* is the Weber number, which is the ratio between the inertial force exerted on the bacterial particle and the particle surface tension force. *Oh* is the Ohnesorge number, which is the ratio between the viscous forces and the surface tension force. v_{p_i} and v_{g_i} are the particle and gas velocity in the *x*-direction (i.e., direction of flow along centerline), respectively. Therefore, bacterial membrane break-up is inferred by computing the relative velocity $(v_{p_i}-v_{g_i})$ of the bacterium and the maximum acceleration achieved. The critical acceleration conditions that

Author's personal copy

Table 3
Cell properties for *E. coli* and *B. atropheus* (Chen et al., 2010; Zinin et al., 2005) and critical shock properties needed to induce bacterial break-up.

Cell	Gram stain	State	d_p (μm)	σ (N/m)	a_c (m/s^2)	We_c
E. coli	−ve	Vegetative	1	7.5×10^{-3}	3.0×10^{8}	1.4×10^{1}
B. atropheus	+ve	Spore	0.5	9.6×10^{-2}	1.6×10^{10}	1.3×10^{1}
B. atropheus	+ve	Spore	1	9.6×10^{-2}	3.9×10^{9}	1.2×10^{1}

Values are reported for both 0.5 μm and 1 μm for spores.

satisfy the conditions for break-up are met for $\chi=0.11$; however, the conditions for the Weber number are not. As reported in Section 4.2 and in previous work (Sislian et al., 2010), cells will still break-up under non-critical Weber number conditions; which points to the conservative nature of the Weber number conditions. In this study, only the effect of Rayleigh–Taylor instabilities is considered.

Bacterial cells with a lower surface tension and larger diameters require lower accelerations to break-up. Vegetative *E. coli* cells have an order of magnitude lower surface tension than *B. atropheus* spores and therefore a lower critical acceleration (see Table 3). It is important to note that the surface tension values reported in Table 3 are derived from the turgor pressure (Zinin et al., 2005) and contact angle (Chen et al., 2010). However, the surface tension can vary with deformation generated by fluid flow over the cell membrane. Such a variation of the cell surface tension under fluid flow may limit the accuracy of the critical acceleration predictions of Table 3. In such a case, more accurate models of the variation of cell surface tension under stress generated by the fluid flow (similar to the works of Kleinig and Middelberg, 1996, 1998; Smith et al., 1998; Zhang et al., 1992) should be utilized and combined with the fluid flow and particle motion models developed here to make accurate critical acceleration predictions. Furthermore, surface tension varies from cell-to-cell in the same culture introducing a distribution of critical accelerations (Smith et al., 2000). An average surface tension value is used in the current study to predict the experimental break-up of cells as discussed in Section 4. Previous work (Kleinig and Middelberg, 1998) has demonstrated for the first time the use of inertial forces (expressed in terms of the Weber number and acceleration) in achieving cell break-up in the context of a high-pressure homogenization system.

4. Experimental results and discussion

4.1. Flow cytometry results

Fig. 6 shows a representative set of raw data obtained using the protocols described in Section 2.3. A total of 18 experiments were performed with six different starting spore suspensions. In the left plots, the side scatter (SSC) versus the forward scatter (FSC) (see Fig. 6) is a measure of the relative particle sizes. The S gate indicates the population of spores. The right plots in Fig. 6 show the red (FL2-H) versus green (FL1-H) fluorescence emission (see Section 2.3) of the spores in gate S. The negative (Fig. 6-a and b) and positive (Fig. 6-c and d) control define the live and dead cell regions in the FL2-H versus FL1-H plots. The live regions are indicated by the gate L and the dead by D. The fraction of live cells (L/S) is determined by dividing the number of spores in gate L by the total number of spores in gate S ($S=L+D$). The average value of the fraction of live cells (L/S) from all 18 experiments is presented in Fig. 7 and Table 4. L/S is not the true measure of the effect of the aerodynamic shock on bacterial aerosol since it only measures intact cells. The overall neutralization $1-f_I$ or fraction of cells remaining intact after the effect of the impactor f_I is calculated through a mass balance on the experimental system and is discussed in Section 4.2.

Using a two-tailed t-test with unequal variance, the fraction of live cells for the negative control and $\chi=0.98$ is equal with a $p>95\%$ (see Table 4). However, the mean fractions of live cells are unequal for $\chi=0.98$, 0.50, and 0.11 ($L/S_{0.98}>L/S_{0.50}>L/S_{0.11}$) with a $p>95\%$. In our previous work with *E. coli*, $L/V_{0.98}>L/V_{0.50}=L/V_{0.11}$ (where $V=L+D$ represents the vegetative cells gate) with a $p>95\%$ (Sislian et al., 2010). The results are discussed in Section 4.2 in comparison to the fraction of cells that remain alive after the shock (f_I), which accounts for the total mass balance in the system.

4.1.1. Lysozyme treatment results

The effect of lysozyme on spores (Fig. 8-c and d) is compared to the effect of lysozyme on vegetative *B. atropheus* cells (Fig. 8-g and h) in order to confirm the presence of spores in the starting suspensions. The live (L) and dead (D) gates were set by running a positive control for both spore and vegetative cells (not shown in Fig. 8). Ethanol is used as a positive control for vegetative cells as in previous work (Sislian et al., 2010). The V gate indicates the vegetative cell population versus the S gate for the spore population. No shift in the spore population is seen after treatment with lysozyme in Fig. 8-a and c. For vegetative *B. atropheus* cells the forward scatter decreases (Fig. 8-e versus g) after lysozyme treatment indicating smaller cell sizes or lysis. Furthermore, the vegetative cells treated with lysozyme shift to the D gate. Comparing both the scatter and fluorescence plots for spores and vegetative cells it is clear that the starting spore suspensions are not affected by lysozyme treatment. The fraction of live spore cells (L/S) after lysozyme treatment is 0.868 ± 0.253 (four measurements) and 0.020 ± 0.114 (two measurements) for vegetative cells (L/V) (see Fig. 9). These values are statistically unequal with $p>95\%$. The mean value of L/S for the starting spore suspension and spores treated with lysozyme were statistically equal ($p>95\%$) which suggests that most of the nebulized cells were indeed spores.

4.2. Effect of the aerodynamic shock on B. atropheus spores

The fraction of cells that remain alive after the effect of impactor operation (f_I) provides a quantitative measure of aerodynamic shock effect when compared to the operation of the impactor under non-critical acceleration conditions. Fluorescence flow cytometry measurements (see Section 2.3) and computational particle tracking (see Section 3.2.2) are used to calculate f_I using the following expression (Sislian et al., 2010):

$$f_I=\frac{n_c}{n_c'}=\frac{n_c}{n_{sl}\phi\eta} \tag{9}$$

where n_c is the number of live cells collected after the impactor operation as measured by flow cytometry (see Section 4.1) and is equal to the cells in gate L multiplied by the volume of PBS remaining in the collection tube. n_c' is the number of live cells that would be collected if the impactor operation had no effect. n_c' cannot be determined from direct measurements because of the

Author's personal copy

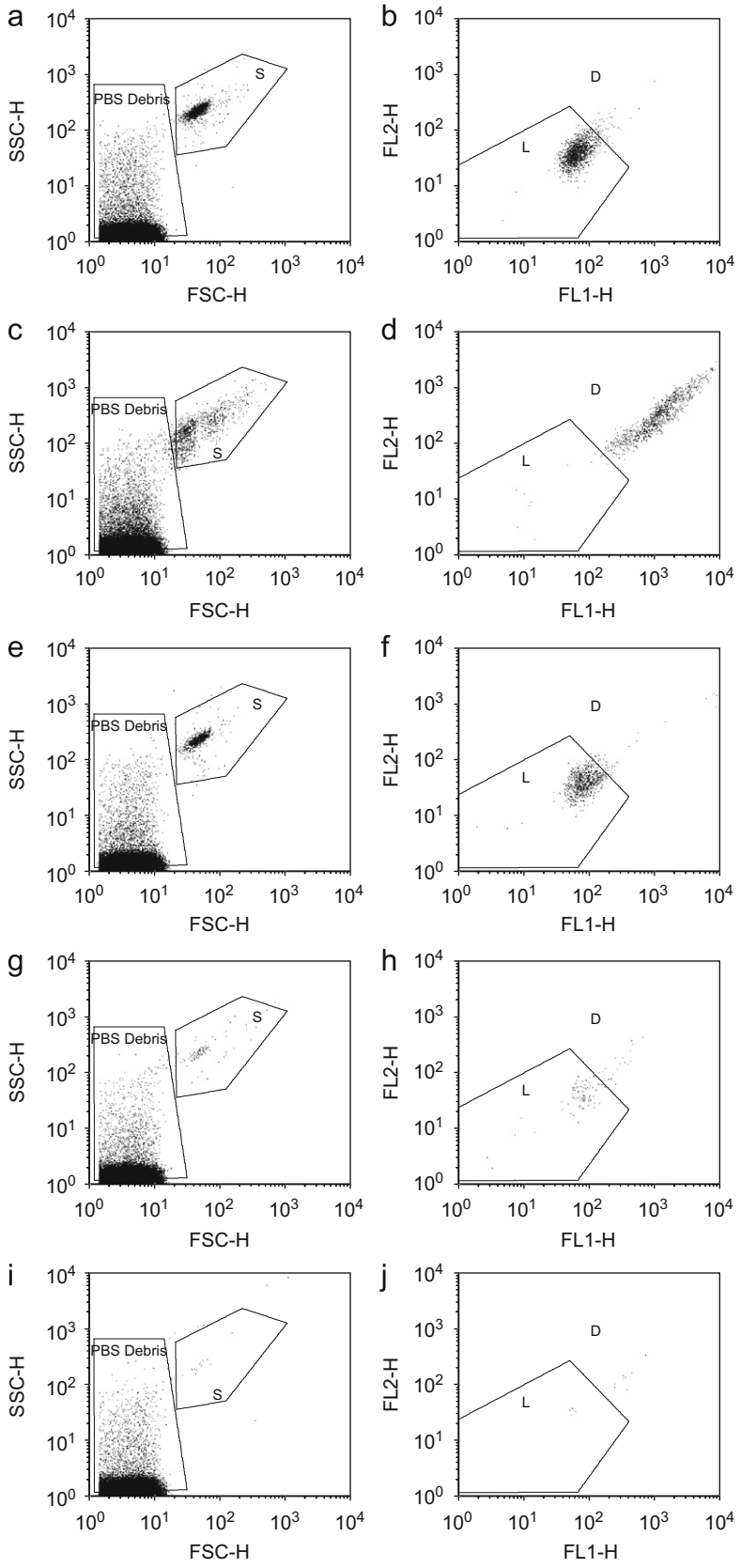

Fig. 6. (Left) Side-scatter versus forward-scatter plot of all particles in the flow cytometer. The S gate indicates the particle sizes which represent intact spores. PBS debris indicates the debris population. (Right) Red fluorescence (FL2-H) versus green fluorescence (FL1-H) of gated cells in the left side plots. The L gate represents the live cells and the D gate represents the dead cells. (a,b) Spore suspension in PBS at $OD_{600}=0.05$, (c,d) spore suspension after exposure to heat, (e,f) cells collected after passing impactor operated at $\chi=0.98$, (g,h) $\chi=0.50$ and (i,j) $\chi=0.11$.

Author's personal copy

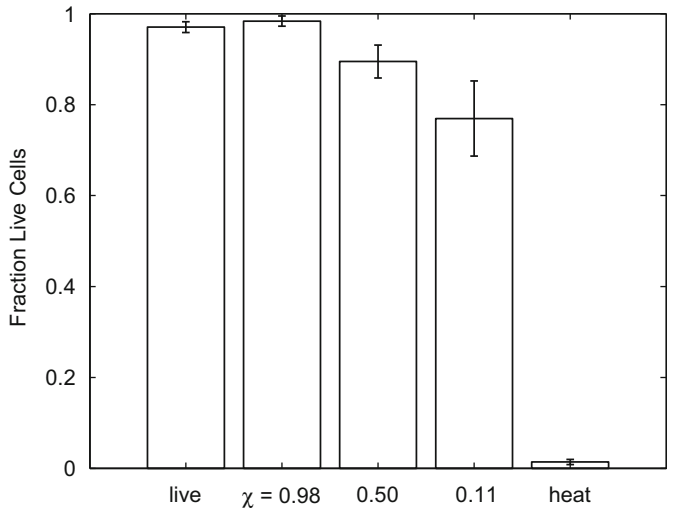

Fig. 7. Fraction of live cells in different collected samples (L/S). All experiments start with a measurement of the fraction of live cells in the cell culture (live), and the negative control (heat). The cells that pass through the impactor system and then collected in the collection tube at $\chi = 0.98$, 0.50, and 0.11 with $P_0 = 1$ atm. Error bars show the 95% confidence interval using a normal distribution for 18 measurements per sample.

Table 4
Measured fraction of live cells (L/S) and the fraction of spores surviving the shock (f_l) for both $d_p = 0.5$ and 1 μm.

Condition	L/S	f_l(0.5 μm)	f_l(1 μm)
−ve control	0.971 ± 0.012	–	–
$\chi = 0.98$	0.983 ± 0.011	0.715 ± 0.235	0.531 ± 0.176
$\chi = 0.50$	0.895 ± 0.036	0.033 ± 0.011	0.022 ± 0.008
$\chi = 0.11$	0.765 ± 0.082	0.030 ± 0.010	0.020 ± 0.007
+ve control (heat)	0.014 ± 0.006	0.008 ± 0.003	–

The f_l for the +ve control is not size dependent but is presented under the 0.5 μm column for convenience.

aerodynamic shock effect. A mass balance accounting for the losses, shown in Fig. 1, has been used where ϕ is the particle loss before the impactor (see Section 2.1.3) and η is the particle collection efficiency (see Section 3.2.2). n_c' becomes $n_{sl}\phi\eta$. n_{sl} is the number of live cells in suspension as measured by flow cytometry (see Section 4.1) and is equal to the cells in gate L multiplied by 1 mL (volume of nebulized suspension). The particle losses before the impactor are calculated in Section 2.1.3 and are given as $\phi = 0.088 \pm 0.029$. The collection efficiency (η) for both 0.5 and 1 μm spores of the impactor system is given in Table 2. As presented in Fig. 10 and Table 4, f_l decreases with increasing η (see Remark 2). Both f_l values are calculated and reported in Table 4 and Fig. 10. A detailed derivation of Eq. (9) is shown in our previous work (Sislian et al., 2010).

The critical acceleration (a_c) for 0.5 and 1 μm spores are 1.6×10^{10} and 3.9×10^9 m/s^2, respectively (see Table 3). At $\chi = 0.98$, the maximum computed acceleration in the experimental impactor is 1.7×10^6 m/s^2 (see Table 2). The computed accelerations are three orders of magnitude lower than the critical accelerations required for break-up. The computational results therefore predict that break-up of spores is not achieved under these conditions. Experimental values of f_l for $\chi = 0.98$ closely match the predictions with 0.715 ± 0.235 fraction of the cells surviving the impactor operation. Additionally, for $\chi = 0.11$, where the aerodynamic shock is strongest, spores reach maximum accelerations of 5.9×10^9 and 5.0×10^9 m/s^2 for 0.5 and 1 μm spores, respectively (see Table 2). The critical acceleration for 0.5 μm spores is 63% greater (less than an order of magnitude) than the computed accelerations in the impactor. The computations provide insight into the flow structures in the impactor system and are not exact representations of the real fluid flow. Therefore, a 63% difference in value is not significant and is reflected in the experimental f_l values for $\chi = 0.11$ as presented in Table 4 and Fig. 10. The same argument cannot be made for $\chi = 0.50$ where the computed a_{max} is an order of magnitude lower than a_c, yet f_l shows experimental break-up of the cells. As mentioned in Section 3.3, the values for surface tensions are calculated either from turgor pressure or contact angle measurements and might not reflect the actual surface tensions under shear conditions. The surface tension values of spores under shear can change the calculated critical accelerations (see Section 3.3). However, obtaining these values is outside the scope of this work. Therefore, the computational along with experimental results provide a framework for assessing the effect of the aerodynamic shock on the spores rather than an exact estimate. For both 0.5 and 1 μm cells, f_l at $\chi = 0.11$ is less than f_l at $\chi = 0.50$ with $p > 95\%$. For the non-shock case the f_l is significantly higher. The same trends were observed in our previous work with *E. coli* (Sislian et al., 2010).

As discussed in Section 4.1, *B. atropheus* spores that survive break-up in the impactor system and are collected in the deceleration tube are more likely to be alive than *E. coli* vegetative cells ($L/S_{0.11} > L/V_{0.50}$). The data indicate that the spore coat is more resistant to membrane damage if the particle remains intact (see Remark 1). The damage increases as the χ decreases while in vegetative experiments the damage is already at a maximum at $\chi = 0.5$ (Sislian et al., 2010). In addition, f_l is equal to both $\chi = 0.11$ and 0.5. Although, the same number of cells are breaking up the remaining cells are weaker as the acceleration is higher. Operating the impactor at lower χ (i.e., higher accelerations) can give more insight into the mechanism of break-up for both vegetative cells and spores. We expect f_l values to be lower as cells that currently survive the shock get weaker and break-up.

Remark 1. The accelerations calculated in Section 3.2 are centerline accelerations. In reality the bacterial particles experience a distribution of accelerations with the maximum at the centerline. For $\chi = 0.5$ the accelerations away from the centerline can be at values where the spore coat of intact cells is not affected.

Remark 2. In order to calculate the exact value for f_l, the average collection efficiency has to be calculated from the particle size distribution of the spore suspension. More measurements are required to obtain an accurate size distribution. For example, an aerosol particle size analyzer could be used. However, the focus of this study is to show the range of possible f_l values, instead of a very accurate value. This range is sufficient to determine the effect of the aerodynamic shock and for comparing the experimental results to computational results.

5. Conclusions

The aerodynamic shock was experimentally shown to cause break-up of *B. atropheus* spores at $\chi = 0.11$ and 0.50. The study provides a framework that yields the parameters needed to guide designs of systems that can neutralize spore aerosols at their release. The computational model predicts the break-up of the spores at $\chi = 0.11$ where accelerations in the aerodynamic shock can reach values higher than the a_c ($3.9 \times 10^9 - 1.6 \times 10^{10}$ m/s^2). The experimental results confirm the predictions with $f_l = 0.030 \pm 0.010$. The model also predicts the survival of spores at accelerations of 10^6 m/s^2 by operating the impactor at $\chi = 0.98$. This prediction was also confirmed experimentally with

Author's personal copy

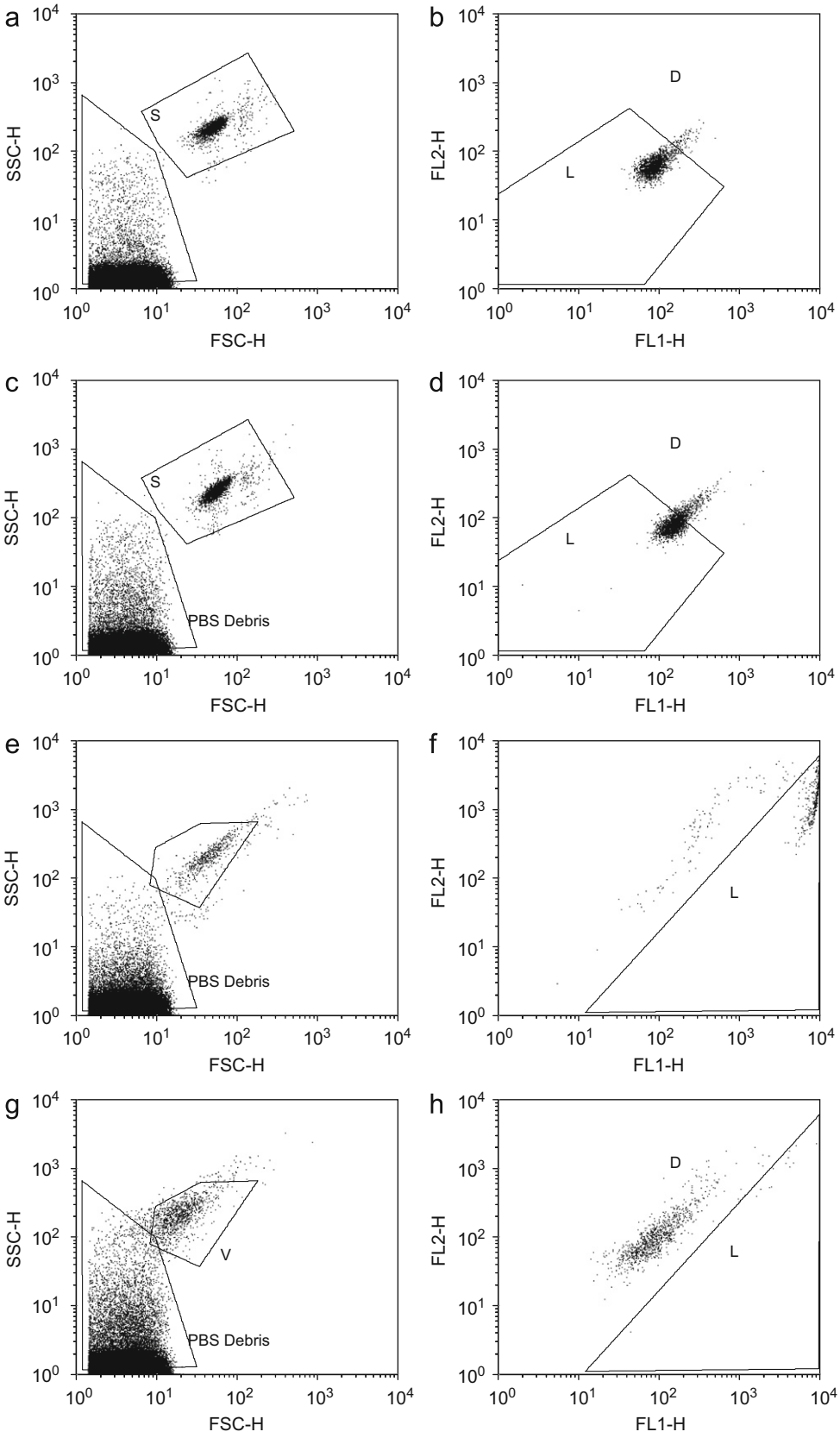

Fig. 8. (Left) Side-scatter versus forward-scatter plot of all particles in the flow cytometer. The S gate indicates the particle sizes which represent intact spores. The V gate represents the intact vegetative cells. PBS debris indicates the debris population. (Right) Red fluorescence (FLH-2) versus green fluorescence (FLH-1) of gated cells in the left side plots. The L gate represents the live cells and the D gate represents the dead cells. (a,b) Spore suspension in PBS, (c,d) spore suspension with lysozyme treatment, (e,f) vegetative suspension in PBS and (g,h) vegetative suspension with lysozyme treatment.

Author's personal copy

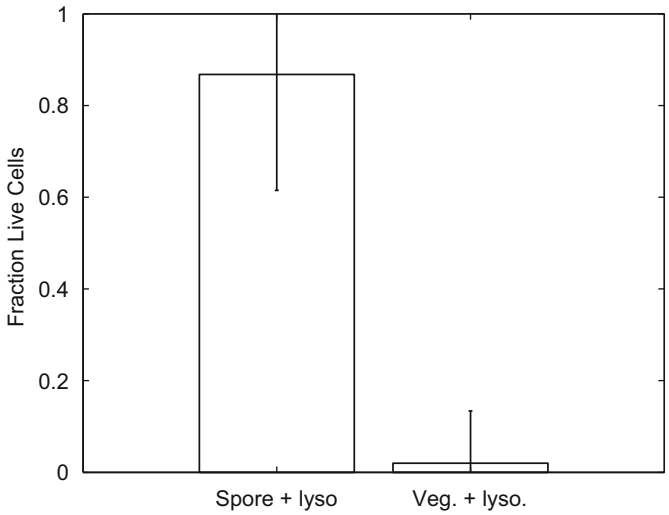

Fig. 9. Fraction of live cells (L/S) after lysozyme treatment for both spores and vegetative cells. Error bars show the 95% confidence interval using a normal distribution for four measurements for spores and two measurements for vegetative cells.

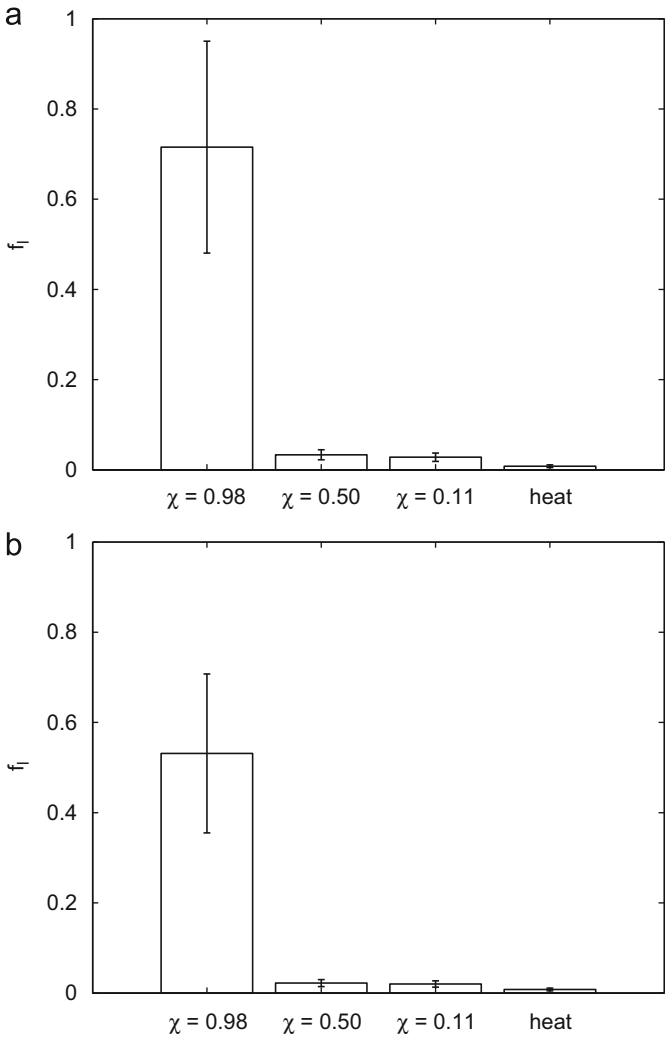

Fig. 10. Fraction of cells that remain alive after the effect of impactor operation (f_l) and after exposure to heat. Live cells in these samples are compared to live cells in the negative control by accounting for losses before the impactor and for the collection efficiency of the impactor for (a) $d_p = 0.5\,\mu m$ and (b) $d_p = 1\,\mu m$. Error bars show the 95% confidence interval using a normal distribution for 18 measurements per sample.

$f_l = 0.715 \pm 0.235$. The critical accelerations were computed using static calculations of surface tension. When surface tension values under shear conditions become available for *B. atropheus* spores, the predictions can be adjusted using the framework provided in this work and previous work (Sislian et al., 2010, 2009).

Nomenclature

a_c	critical bacterial acceleration, m/s^2
A_p	projected area of particle, m^2
C_D	drag coefficient
d	nozzle diameter, m
d_p	particle diameter, m
D	particle diffusion coefficient, m^2/s
D_s	diameter of tubes leading to impactor system, m
f_l	fraction of cells that remain alive after the effects of acceleration
k	turbulent kinetic energy, Nm/kg
L	length of tubes leading to impactor system, m
m_p	particle mass, kg
n_c	experimentally measured number of live cells
n_i	number of particles entering the impactor
n_n	number of cells nebulized
n_{sl}	number of live cells after nebulization
n_c'	number of live cells under assumption of no break-up
Oh	Ohnesorge number
p	static pressure of gas, atm
P_0	upstream stagnation pressure, atm
P_1	downstream stagnation pressure, atm
P_n	nebulization pressure, atm
Q_g	volumetric flow rate of gas in tubes leading to impactor system, m^3/s
t_L	Lagrangian time interval, s
U_g	velocity of gas in tubes leading to impactor system, m/s
v_p	particle velocity, m/s
v_g	gas velocity, m/s
We	Weber number
We_c	critical Weber number
x	plate to nozzle distance, m

Greek letters

ε	rate of turbulent dissipation, m^2/s^3
ζ	normally distributed random variable
η	impactor collection efficiency
μ_g	dynamic viscosity of gas, N/m^{2}s
ρ_g	gas density, kg/m^3
ρ_p	particle density, kg/m^3
σ	bacterial surface tension, N/m
τ_ε	lifetime of eddies, s
ϕ	fraction of particles not lost before entering impactor
χ	downstream to upstream pressure ratio

Acknowledgements

This work has been supported by the Defense Threat Reduction Agency (DTRA) under Grant number HDTRA1-07-0012. The authors would like to acknowledge the late Prof. Sheldon K. Friedlander for initiating the project and for advising Patrick R. Sislian at the early stage of his work. The authors would also like to thank Prof. Jennifer A. Jay for providing unrestricted access to

Author's personal copy

the fluorescence microscope. Flow cytometry was performed in the UCLA Jonsson Comprehensive Cancer Center (JCCC) and Center for AIDS Research Flow Cytometry Core Facility that is supported by National Institutes of Health awards CA-16042 and AI-28697, and by the JCCC, the UCLA AIDS Institute, and the David Geffen School of Medicine at UCLA.

References

Alvi, F.S., Ladd, J.A., Bower, W.W., 2002. Experimental and computational investigation of supersonic impinging jets. AIAA Journal 40 (4), 599–609.

Berney, M., Hammes, F., Bosshard, F., Weilenmann, H.U., Egli, T., 2007. Assessment and interpretation of bacterial viability by using the live/dead baclight kit in combination with flow cytometry. Applied and Environmental Microbiology 73 (10), 3283–3290.

Chandrasekhar, S., 1961. Hydrodynamic and hydromagnetic stability. In: The International Series of Monographs on Physics first ed. Clarendon Press, Oxford.

Chen, G., Driks, A., Tawfiq, K., Mallozzi, M., Patil, S., 2010. *Bacillus anthracis* and *Bacillus subtilis* spore surface properties and transport. Colloids and Surfaces B: Biointerfaces 76 (2), 512–518.

Clift, R., Grace, J.R., Weber, M.E., 1978. Bubbles, Drops, and Particles. Academic Press, New York.

Conn, H.J., 1930. The identity of *Bacillus subtilis*. The Journal of Infectious Diseases 46 (4), 341–350.

Cortezzo, D.E., Koziol-Dube, K., Setlow, B., Setlow, P., 2004. Treatment with oxidizing agents damages the inner membrane of spores of *Bacillus subtilis* and sensitizes spores to subsequent stress. Journal of Applied Microbiology 97 (4), 838–852.

Delamora, J.F., Hering, S.V., Rao, N., McMurry, P.H., 1990. Hypersonic impaction of ultrafine particles. Journal of Aerosol Science 21 (2), 169–187.

Delamora, J.F., Rao, N., McMurry, P.H., 1990. Inertial impaction of fine particles at moderate Reynolds-numbers and in the transonic regime with a thin-plate orifice nozzle. Journal of Aerosol Science 21 (7), 889–909.

Fitch, J., 2005. Review of testing and evaluation methodology for biological point detectors. Technical Report, The National Academies Press.

Friedlander, S.K., 2000. Smoke, Dust, and Haze: Fundamentals of Aerosol Dynamics, second ed. Topics in Chemical Engineering. Oxford University Press, New York.

Fritze, D., Pukall, R., 2001. Reclassification of bioindicator strains *Bacillus subtilis* dsm 675 and *Bacillus subtilis* dsm 2277 as *Bacillus atrophaeus*. International Journal of Systematic and Evolutionary Microbiology 51, 35–37.

Harwood, C., Cutting, S., 1990. Molecular biological methods for bacillus. In: Modern Microbiological Methods, first ed.. John Wiley & Sons, Chichester.

Hering, S.V., Flagan, R.C., Friedlander, S.K., 1978. Design and evaluation of new low-pressure impactor.1. Environmental Science and Technology 12 (6), 667–673.

Hering, S.V., Friedlander, S.K., Collins, J.J., Richards, L.W., 1979. Design and evaluation of a new low-pressure impactor.2. Environmental Science and Technology 13 (2), 184–188.

Hinds, W., 1999. Aerosol Technology: Properties, Behavior and Measurement of Airborne Particles, second ed. John Wiley & Sons, New York.

Hinze, J.O., 1975. Turbulence, second ed. McGraw-Hill Series in Mechanical Engineering. McGraw-Hill, New York.

Horneck, G., Stoffler, D., Eschweiler, U., Hornemann, U., 2001. Bacterial spores survive simulated meteorite impact. Icarus 149 (1), 285–290.

Joseph, D.D., Belanger, J., Beavers, G.S., 1999. Breakup of a liquid drop suddenly exposed to a high-speed airstream. International Journal of Multiphase Flow 25 (6–7), 1263–1303.

Jurcik, B.J., Brock, J.R., Trachtenberg, I., 1989. A study of low-pressure particle impaction processes. Journal of Aerosol Science 20 (6), 701–711.

Kleinig, A.R., Middelberg, A.P.J., 1996. The correlation of cell disruption with homogenizer valve pressure gradient determined by computational fluid dynamics. Chemical Engineering Science 51 (23), 5103–5110.

Kleinig, A.R., Middelberg, A.P.J., 1998. On the mechanism of microbial cell disruption in high-pressure homogenisation. Chemical Engineering Science 53 (5), 891–898.

Laflamme, C., Lavigne, S., Ho, J., Duchaine, C., 2004. Assessment of bacterial endospore viability with fluorescent dyes. Journal of Applied Microbiology 96 (4), 684–692.

Laskin, A.I., Lechevalier, H.A., 1974. CRC Handbook of Microbiology. vol. 1, CRC Press, Cleveland.

Liepmann, H.W., Roshko, A., 2001. Elements of Gas Dynamics. Dover Books on Engineering. Dover Publications, New York.

Lundbeck, H., Skoldber, O., 1963. Effect of pressure waves on bacteria suspended in water. Biotechnology and Bioengineering 5 (3), 167–184.

Powell, A., 1988. The sound-producing oscillations of round underexpanded jets impinging on normal plates. Journal of the Acoustical Society of America 83 (2), 515–533.

Shapiro, A.H., 1953. The Dynamics and Thermodynamics of Compressible Fluid Flow. The Ronald Press Company, New York.

Sislian, P.R., Pham, D., Zhang, X., Li, M., Mädler, L., Christofides, P.D., 2010. Bacterial aerosol neutralization by aerodynamic shocks using an impactor system: experimental results for *E. coli* and analysis. Chemical Engineering Science 65 (4), 1490–1502.

Sislian, P.R., Zhang, X., Li, M., Pham, D., Mädler, L., Christofides, P.D., 2009. Bacterial aerosol neutralization by aerodynamic shocks using a novel impactor system: design and computation. Chemical Engineering Science 64 (9), 1953–1967.

Smith, A.E., Moxham, K.E., Middelberg, A.P.J., 1998. On uniquely determining cell-wall material properties with the compression experiment. Chemical Engineering Science 53 (23), 3913–3922.

Smith, A.E., Zhang, Z.B., Thomas, C.R., Moxham, K.E., Middelberg, A.P.J., 2000. The mechanical properties of *Saccharomyces cerevisiae*. Proceedings of the National Academy of Sciences of the United States of America 97 (18), 9871–9874.

Stewart, S.L., Grinshpun, S.A., Willeke, K., Terzieva, S., Ulevicius, V., Donnelly, J., 1995. Effect of impact stress on microbial recovery on an agar surface. Applied and Environmental Microbiology 61 (4), 1232–1239.

Stuart, A.L., Wilkening, D.A., 2005. Degradation of biological weapons agents in the environment: implications for terrorism response. Environmental Science & Technology 39 (8), 2736–2743.

Tang, J.W., 2009. The effect of environmental parameters on the survival of airborne infectious agents. Journal of the Royal Society Interface 6, S737–S746.

Teshima, K., Ohshima, T., Tanaka, S., Nagai, T., 1995. Biomechanical effects of shock-waves on *Escherichia-coli* and lambda-phage DNA. Shock Waves 4 (6), 293–297.

Vitko, J., 2005. Sensor systems for biological agent attacks: protecting buildings and military bases. Technical Report, The National Academies Press.

Willeke, K., Baron, P.A., 2001. Aerosol Measurement: Principles, Techniques, and Applications. Wiley-Interscience, New York.

Zhang, Z., Ferenczi, M.A., Thomas, C.R., 1992. A micromanipulation technique with a theoretical cell model for determining mechanical-properties of single mammalian-cells. Chemical Engineering Science 47 (6), 1347–1354.

Zinin, P.V., Allen, J.S., Levin, V.M., 2005. Mechanical resonances of bacteria cells. Physical Review E 72 (6), 061907.1–061907.10.